# Fabricating fiber Bragg gratings based on composite manufacturing methods

QING TAO[2,3], CHENCHEN WU[2], XIAOLIANG WANG[2], YUNLONG SONG[2], CHONGCHONG WANG[2], JIAN CHENG[2], DUN LIU[2,*], BOWEN LU[1,*]
[1]State Key Laboratory of Optical Fiber and Cable Manufacture Technology (YOFC), Wuhan 430068, China
[2]Laser Group, School of Mechanical Engineering, Hubei University of Technology, Wuhan 430068, China
[3]Hubei Key Laboratory of Modern Manufacturing Quantity Engineering, School of Mechanical Engineering, Hubei University of Technology, Wuhan 430068, Hubei, China

In this paper, simultaneous spatiotemporal focusing femtosecond laser combined with acupuncture method is proposed. Two gradient index fiber Bragg gratings are designed and fabricated. Their center wavelengths are 980 nm and 1080 nm, bandwidths are 0.23 nm and 0.49 nm, periods are 0.32 μm and 0.36 μm. Testing results show that center wavelength of G1 Bragg grating is 979.372 nm with bandwidth of 0.25 nm. The center wavelength of G2 Bragg grating is 1080.1 nm with bandwidth of 0.52 nm. And, their reflectivity is greater than 99%. The actual results meet the design requirements.

## 1. Introduction

Fiber Bragg gratings (FBG) [1-3] are widely used in automation processing systems due to their excellent performance such as anti-electromagnetic interference, high resolution, small size, and long-distance transmission. Classical fabricating technology of FBG uses phase mask technique [4-7] with fixed grating length. And fabricating FBG uses excimer laser [8-10]. However, this method damages the coating layer of optical fiber, and period and length of Bragg grating are fixed. Ultra-short pulse laser inducing [11-12] is a technology that can effectively improve the accuracy of microstructure fabrication. It has the advantage of high peak power. And it is suitable for processing various hard and brittle materials.

Some Bragg gratings can be fabricated in optical fibers by using femtosecond lasers with phase masks or point by point etching techniques [13-14]. Their characteristics are directly affected by laser energy, inducing time, focusing numerical aperture, etc. Moreover, interaction mechanism between femtosecond laser and various fiber materials still needs to be researched. For example, reasons for ultrafast laser-induced refractive index change in silica [15-16] include stress, densification [17-18], color center [19-20], and cumulative heating [21-22]. Generally, low energy laser can lead to positive refractive index change in the Type I structure related to color center theory. While laser energy exceeds damage threshold, it will typically produce Type II structure related to stress and densification. Therefore, there is increasing research on femtosecond lasers and various fiber materials.

Classical laser focusing methods cannot break through the diffraction limit for nanoscale fabrication. Simultaneous spatiotemporal focusing femtosecond laser (STFFL) [23-24] can compensate this deficiency. It is used to draw lines or points in the core layer of fiber for nanoscale process. And it does not damage the coating layer of optical fiber. Moreover, simultaneous spatiotemporal focusing femtosecond laser combined with acupuncture method is proved to be effective for fabricating fiber Bragg gratings. This new manufacturing method is more flexible. The new method can realize the manufacture of fiber grating more accurately. And the period, length, reflectivity, center wavelength, and bandwidth of fiber Bragg grating can all be adjusted.

So, this new method is used to fabricate two types of special fiber Bragg gratings. Moreover, annealing experiments [25-26] are also executed. These testing results verify the stability and reliability of fiber Bragg gratings. This new method is suitable for the actual manufacturing of fiber Bragg gratings.

## 2. Theoretical analysis

Fiber Bragg grating [27-28] is an optical device that has the function of selecting wavelength. When lights of different wavelengths pass through fiber Bragg gratings, only light that meets the Bragg condition will be reflected. Based on the Maxwell equations, the transverse electric field component transmitted along the fiber can be expressed as,

$$E_t(x,y,z,t) =$$
$$\sum_m [A_m(z) \cdot e^{i\beta z} + B_m(z) \cdot e^{-i\beta z}] \cdot e_{mt}(x,y) e^{-i\omega z} \quad (1)$$

$A_m(z)$ and $B_m(z)$ represent the amplitude of electric field in the forward and backward mode, respectively. $\omega$ is carrier frequency. $i$ is imaginary part. $\beta_m$ is mode propagation constant, which can be expressed as,

$$\beta_m = \frac{2\pi}{\lambda} n_{eff} \quad (2)$$

$\lambda$ is optical wavelength, and $n_{eff}$ is effective refractive index. The variation of effective refractive index in FBG along Z-axis direction can be expressed as,

$$\Delta n_{eff}(z) = \overline{\delta n_{eff}(z)} \left\{ 1 + \upsilon \cos[\frac{2\pi z}{\Lambda} + \varphi(z)] \right\} \quad (3)$$

$\overline{\delta n_{eff}(z)}$ is average effective refractive index modulation, where $v$ is visibility of refractive index variation fringes, $\Lambda$ is grating period, and $\varphi(z)$ is chirp function. For a uniform FBG, $\varphi(z)=0$. When light coupling occurs during transmission, $A_m(z)$ and $B_m(z)$ are,

$$\begin{cases} \dfrac{dA_m(z)}{dz} = \\ i\sum_n A_n K_{mn}^t \cdot e^{i(\beta_n-\beta_m)z} + i\sum_n B_m K_{mn}^t \cdot e^{-i(\beta_n+\beta_m)z} \\ \dfrac{dB_m(z)}{dz} = \\ -i\sum_n A_n K_{mn}^t \cdot e^{2i(\beta_n+\beta_m)z} - i\sum_n B_m K_{mn}^t \cdot e^{-2i(\beta_n-\beta_m)z} \end{cases} \quad (4)$$

$K_{mn}^t$ is lateral coupling coefficient between $m$, $n$ modes, which can be expressed as,

$$K_{mn}^t = \zeta_{mn}^+ + 2\kappa_{mn}[1 + \upsilon \cos(\frac{2\pi z}{\Lambda})] \quad (5)$$

$\zeta_{mn}^+$, $\kappa_{mn}$ are self-coupling coefficients and mutual coupling coefficients of $m$ and $n$ modes, respectively. The self-coupling coefficients are,

$$\zeta_{mn}^+ = \delta + \zeta - \frac{1}{2}\frac{d\varphi}{dz} \quad (6)$$

$\delta$ represents the mismatch between different modes. For uniform FBG, $m=n=1$, self-coupling coefficient and mutual coupling coefficient are respectively,

$$\begin{cases} \zeta_{11}^+ = \dfrac{2\pi}{\lambda}\overline{\delta n_{eff}} \\ \kappa_{11} = \dfrac{\pi}{\lambda}\upsilon\overline{\delta n_{eff}} \end{cases} \quad (7)$$

For single mode FBG with approximately uniform

refractive index distribution, and $\overline{\delta n_{eff}}$ remains unchanged, reflectivity can be expressed as,

$$R = \frac{\sinh^2 \sqrt{(\kappa_{mn}L)^2 - (\zeta_{mn}^+ L)^2}}{-(\zeta_{mn}^+)^2 / \kappa_{mn}^2 + \cosh^2 \sqrt{(\kappa_{mn}L)^2 - (\zeta_{mn}^+ L)^2}} \quad (8)$$

L is FBG length, and when $\zeta_{mn}^+ = 0$, reflectivity has a maximum value.

In this paper, single-mode fiber has a gradient refractive index distribution [29-30] with a maximum refractive index of 1.4669 and a minimum refractive index of 1.4526 in Fig. 1. The diameter of core layer is approximately 9.5 μm, and diameter of lowest refractive index part is about 42.5 μm. The diameter of cladding layer is approximately 128 μm. Two refractive indices are almost same for 980 nm and 1080 nm wavelength.
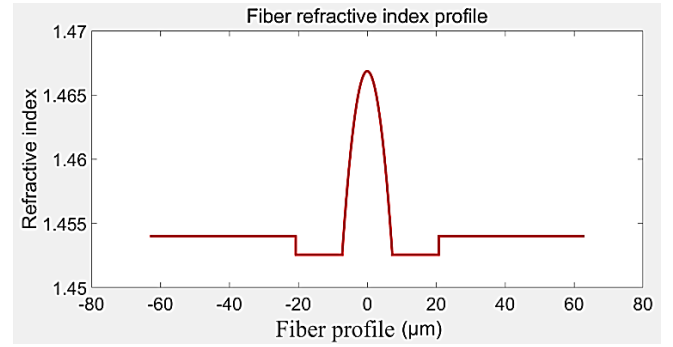


*Fig. 1. Fiber refractive index profile*

Here, fiber Bragg gratings with center wavelength of 980 nm and 1080 nm have been designed, their reflectivity are greater than 99%. The fiber Bragg grating with central wavelength of 980 nm is abbreviated as G1, its period is 0.32 μm, bandwidth is 0.23 nm, and length of fiber Bragg grating is 5 mm in Fig. 2.
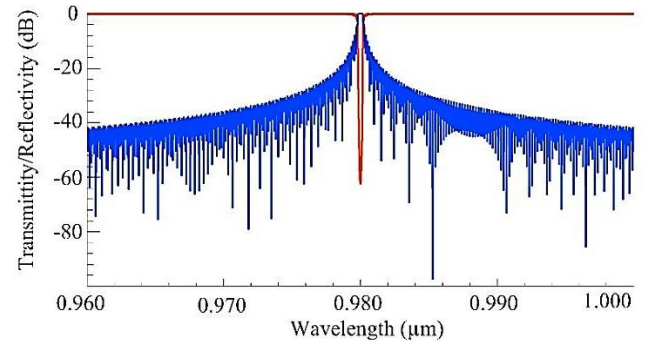


*Fig. 2. Transmittivity and reflectivity of G1 (color online)*

The fiber Bragg grating with central wavelength of 1080 nm is abbreviated as G2, its period is 0.36 μm, bandwidth is 0.49 nm, and length of fiber Bragg grating is also 5 mm in Fig. 3.
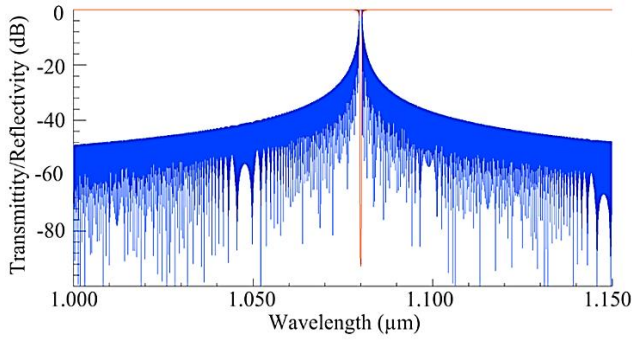
Fig. 3. Transmittivity and reflectivity of G2 (color online)

Above design parameters are specific indicators for two types of fiber Bragg gratings.

## 3. Composite manufacturing method

### 3.1. The principle of simultaneous spatial and temporal focusing

Femtosecond laser pulse has a circular Gaussian distribution, the major axis waist is 4 mm and minor axis waist is also 4 mm. The normalized light field of pulse $A_1$ at the entrance aperture of objective lens is,

$$A_1(x,y,\omega) = \frac{A_0}{\sqrt{\pi}\Omega}\exp(-\frac{(\omega-\omega_0)^2}{\Omega^2})\times$$
$$\exp(-\frac{x-\Delta x(\omega)^2}{2W_x^2})\exp(-\frac{y^2}{2W_y^2}) \quad (9)$$

$A_0$ is optical field amplitude, $\omega_0$ is center carrier frequency, $\omega$ is carrier frequency, $\sqrt{2}\Omega$ is bandwidth of femtosecond pulse, $\sqrt{2}W_x$ and $\sqrt{2}W_y$ are beam waists along major and minor axes, respectively. Linear shift of each spectral component at the entrance aperture can be written as $\Delta x(\omega) \approx \alpha(\omega-\omega_0)$.

The light field behind objective lens is,

$$A_2(x,y,\omega) = A_1(x,y,\omega)\exp(-ik\frac{x^2+y^2}{2f}) \quad (10)$$

$k$ is wave vector and $f = 5mm$ is focal length of objective lens. After propagating $z$, light field can be described by Fresnel diffraction equation,

$$A_3(x,y,z,\omega) = \frac{\exp(ikz)}{i\lambda z}\times\int\int_{-\infty}^{\infty} A_2(\xi,\eta,\omega)\times$$
$$\exp[ik\frac{(x-\xi)^2+(y-\eta)^2}{2z}]d\xi d\eta \quad (11)$$

Performing inversed fourier transformation, light field $A_4$ in the time domain is,

$$A_4(x,y,z,t) = \int_{-\infty}^{\infty} A_3(x,y,z,\omega)\exp(-i\omega t)d\omega \quad (12)$$

Optical intensity is calculated by substituting $z = f$ and $t \approx 0$ into equation (12),

$$I(x,y,z,t) = |A_4|^2 \quad (13)$$

The center wavelength is 400 nm, laser repetition frequency is 1kHz, pulse width is 100 fs, and beam quality factor is $M^2<1.3$. The distance of grating pairs is 830 mm. The input angle of grating pairs is 58º [31-35]. The grating pairs are ruled with 1200 lines /mm. The spectral bandwidth is 8 nm. The resolution of three-dimensional displacement platform is 0.01 μm. The optical spot diameter is about 0.06 μm in Fig. 4.
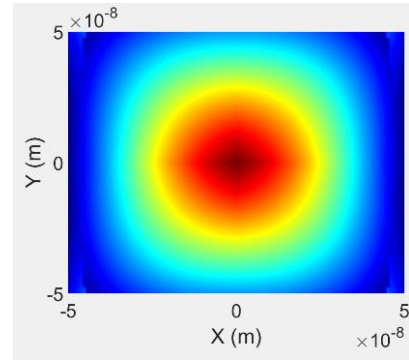


(a) (X-Y direction)
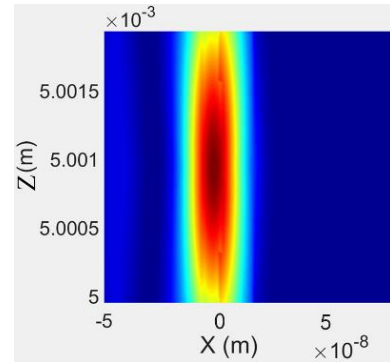


(b) (X-Z direction)
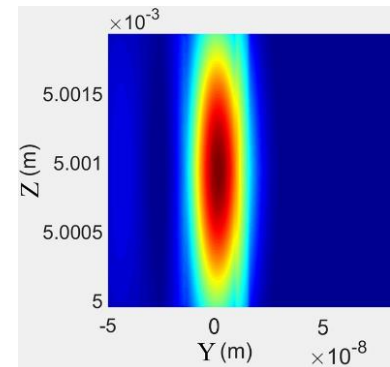


(c) (Y-Z direction)

Fig. 4. Laser focus of femtosecond laser (color online)

### 3.2. Composite manufacturing process

The fiber Bragg gratings are fabricated by STFFL, detail steps are as follows. A glass substrate is immersed into photosensitive resin acrylic ester phenolic resin quaternary ammonium salt solution. And, its surface is fully soaked with the solution. Then, glass substrate is taken out with a clip. The solution is dropped clean. And, glass substrate is air dried. Then, glass substrate with photosensitive coating is completed. Moreover, fiber diameter is measured by a spiral micrometer. Fiber is tightly adhere to the surface of photosensitive glass substrate by clamps. Thereafter, they are placed on a three dimensional displacement platform.

Femtosecond laser passes through an attenuator, laser power is attenuated. The direction of laser transmission changes when laser passes through some reflectors. Shutter controls the on/off state of femtosecond laser. The computer sets a series of parameters for femtosecond laser performance and controls the moving path of three-dimensional displacement platform by programming. The aperture is used to adjust the shape and size of laser beam. The spot diameter is compressed to nanometer level by grating pairs, and a visual system is used to observe the interaction between laser focus and photosensitive material on the glass substrate. The luminance of photoluminescence is observed. Three dimensional displacement platform is slowly moved so that laser focus is perpendicular to the surface of photosensitive glass substrate. When the intensity of photoluminescence attains maximum, laser focus is in full contact with the surface of photosensitive material. And, the distance from surface of photosensitive material to focusing lens is exactly equal to focal length, which is 5 mm. By programming the three-dimensional displacement platform, distance and orientation will be changed between photosensitive glass substrate and focusing lens, laser acupuncture method is used to repeatedly change the refractive index of fiber core point by point to form a fiber Bragg grating. Composite manufacturing method can accurately induce refractive index change in the core layer of optical fibers in Fig. 5. Real-time inducing monitoring system is mainly composed of broadband light source, optical isolator and optical spectrum analyzer. Optical isolator prevents reflected light to damage broadband light source. Single grating separates gaussian beams. Only a small amount of gaussian beam can pass through slit and enter the grating pairs.
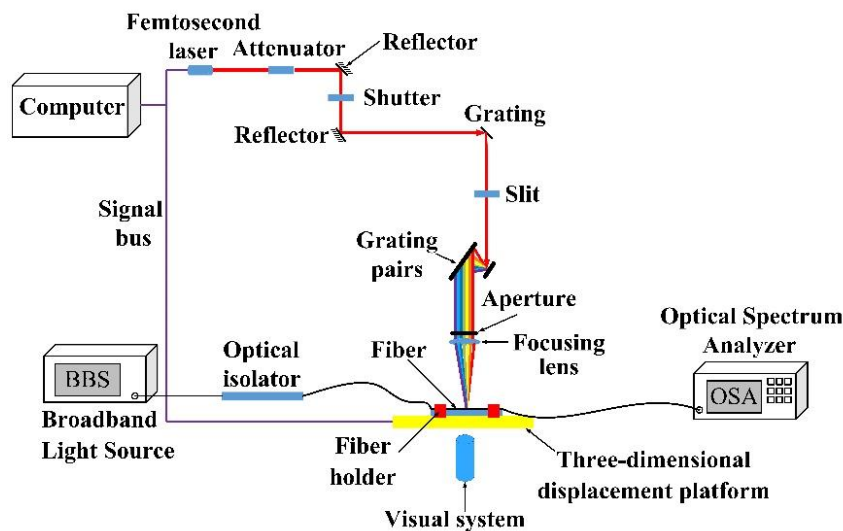


Fig. 5. Femtosecond laser fabricating system (color online)

The statistical relationship between fluence and various indicators have been obtained by a large number of experiments in Fig. 6. For G1 Bragg grating, a fluence between 81 mJ/cm$^2$ and 83 mJ/cm$^2$ has a dense and accurate modulation effects on the center wavelength. Central wavelength lies between 980.39 nm and 980.42 nm every time by laser induction. For G2 Bragg grating, a fluence between 80 mJ/cm$^2$ and 81 mJ/cm$^2$ has an accurate modulation effects on the center wavelength. Central wavelength is between 1080.37 nm and 1080.41 nm every time by laser induction in Fig. 6(a). Similarly, a fluence between 81 mJ/cm$^2$ and 83 mJ/cm$^2$ has an accurate modulation effects on bandwidth for G1 Bragg grating. Bandwidth lies between 0.215 nm and 0.247 nm every time by laser induction. A fluence between 79.5 mJ/cm$^2$ and 81 mJ/cm$^2$ has a dense and accurate modulation effects on bandwidth for G2 Bragg grating. Bandwidth is between 0.52 nm and 0.545 nm every time by laser induction in Fig. 6(b). Another, a fluence between 81 mJ/cm$^2$ and 83.5 mJ/cm$^2$ has an accurate modulation effects on transmission depth for G1 Bragg grating every time. Reflectivity lies between 0.04 dB and 0.08 dB every time by laser induction. A fluence between 79 mJ/cm$^2$ and 81 mJ/cm$^2$ has an accurate modulation effects on transmission depth for G2 Bragg grating every time. Reflectivity is between 0.06 dB and 0.11 dB every time by laser induction in Fig. 6(c). In these statistical results, it can be concluded that optimal fluence is 82 mJ/cm$^2$ for G1 Bragg grating, and optimal fluence is 80 mJ/cm$^2$ for G2 Bragg grating.
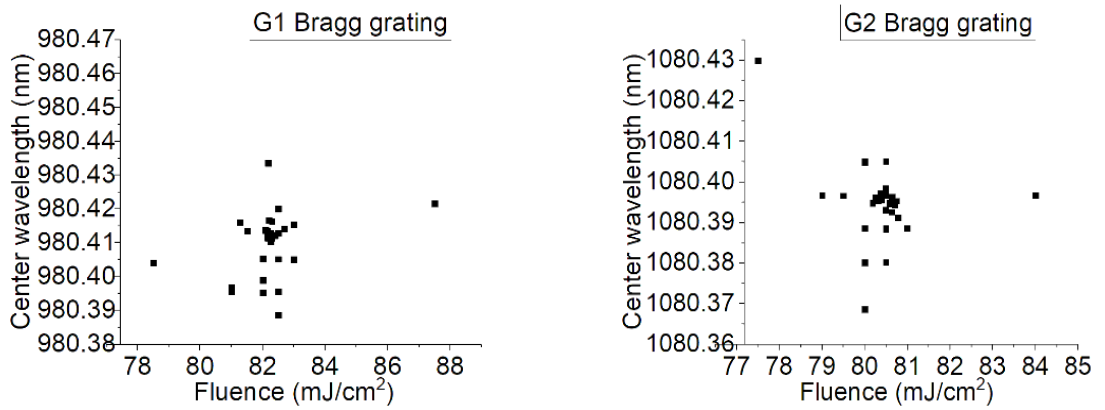
(a)    The scatter diagram of fluence and central wavelengths
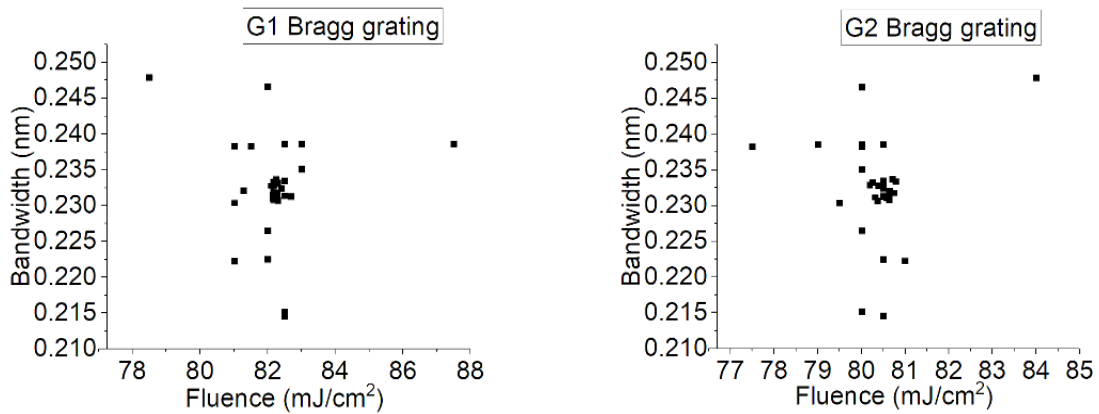


(b)    The scatter diagram of fluence and bandwidths
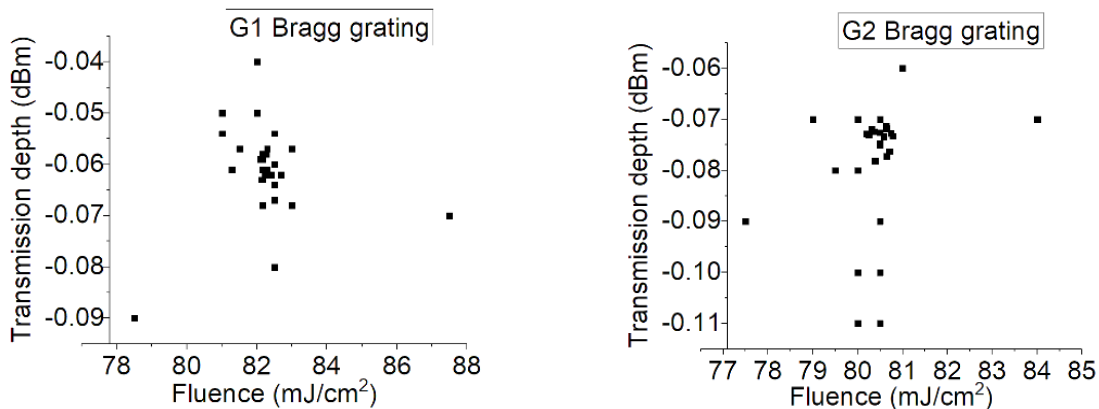


(c)    The scatter diagram of fluence and transmission depths

*Fig. 6. The statistical relationship between fluence and various parameters*

## 4. Results and discussion

When core of fiber is moved to laser focus for G1 Bragg grating, STFFL rapidly induces it for 0.5 seconds. Then, laser switch shuts off. And, fiber detaches quickly

1mm from laser focus along anti-focus-plane direction. Three dimensional displacement platform moves radially 0.03 µm along fiber. Then, laser switch turns on to induce core of fiber for 0.5 seconds. Afterwards, laser shuts off, fiber detaches quickly from laser focus 1mm along

anti-focal-plane direction again. Above process lasts for 4 times. Thereafter, three dimensional displacement platform moves radially 0.16 μm along fiber. Hereto, Bragg grating inducing process for first cycle has been completed. A 5 mm Bragg grating segment can be induced by repeatedly executing above process. The transmissivity and bandwidth are observed in real-time by optical spectrum analyzer. 15625 cycles are performed for each complete induction process for G1 Bragg grating. If displayed indicators do not meet design specifications, laser switch turns off and fiber quickly detaches from laser focus 1 mm along anti-focal-plane direction. Then, three dimensional displacement platform returns radially 5 mm to initiation point in opposite direction. And Bragg grating is re-written until all displayed indicators meet design specifications.

When core of fiber is moved to laser focus for G2 Bragg grating, STFFL rapidly induces it for 0.5 seconds. Then, laser switch shuts off. And, fiber detaches quickly 1mm from laser focus along anti-focus-plane direction. Three dimensional displacement platform radially moves 0.03 μm along fiber. Then, laser switch turns on to induce core of fiber for 0.5 seconds. Afterwards, laser switch shuts off, fiber detaches quickly from laser focus 1 mm along anti-focal-plane direction. Above process lasts for 5 times. Thereafter, three dimensional displacement platform

moves radially 0.18 μm along fiber. Hereto, Bragg grating inducing process for first cycle has been completed. A 5 mm Bragg grating segment can be induced by repeatedly executing above process. The transmissivity and bandwidth are observed in real-time by optical spectrum analyzer. 13889 cycles are performed for each complete induction process for G2 Bragg grating. Similarly, if displayed indicators do not meet design specifications, laser switch turns off and fiber quickly detaches from laser focus 1 mm along anti-focal-plane direction. Then, three dimensional displacement platform radially returns 5 mm to initiation point in opposite direction. And Bragg grating is re-written until all displayed indicators meet design specifications.

Finally, a green light is input into one end of fiber, and optical power is adjusted, induced area of fiber Bragg grating can be found by metallographic microscope in Fig. 7. The diameter of fiber core in the image is approximately 10 μm, and laser inducing paths are clear. Inducing paths are slightly denser in Fig. 7(a). While inducing paths are slightly sparser in Fig. 7(b). The grating length of G1 Bragg grating is about 5.01 mm, the grating length of G2 Bragg grating is about 5.06 mm, which are slightly greater than design values. These are consistent with composite manufacturing process.
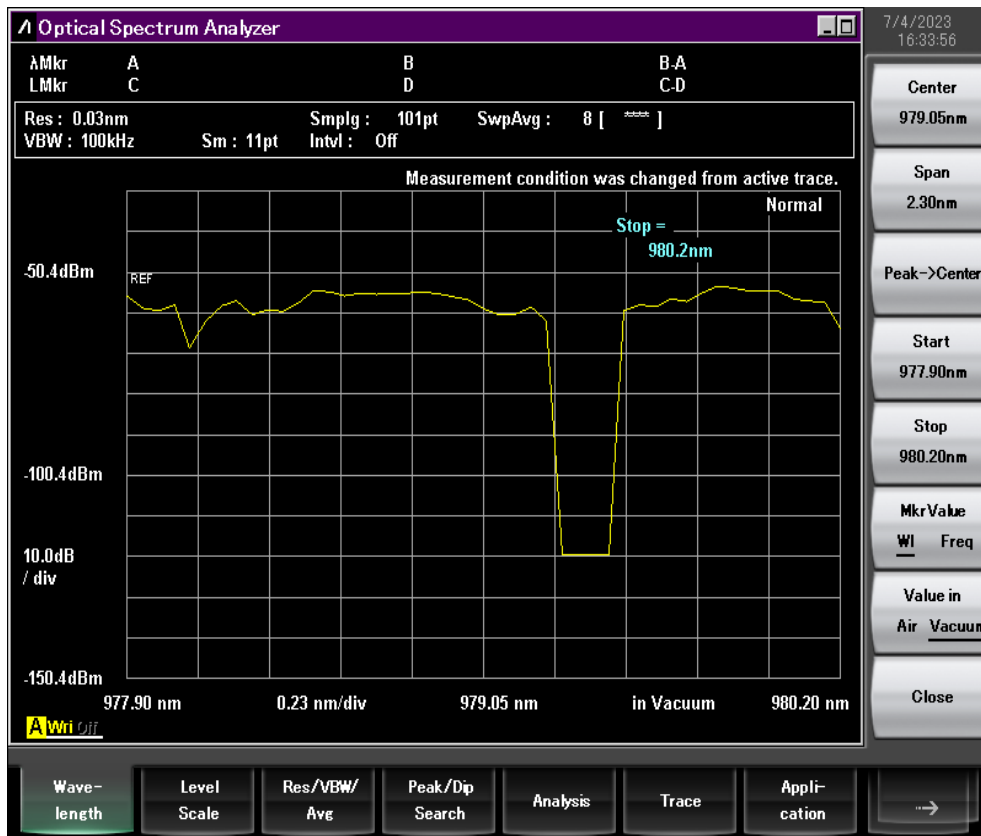


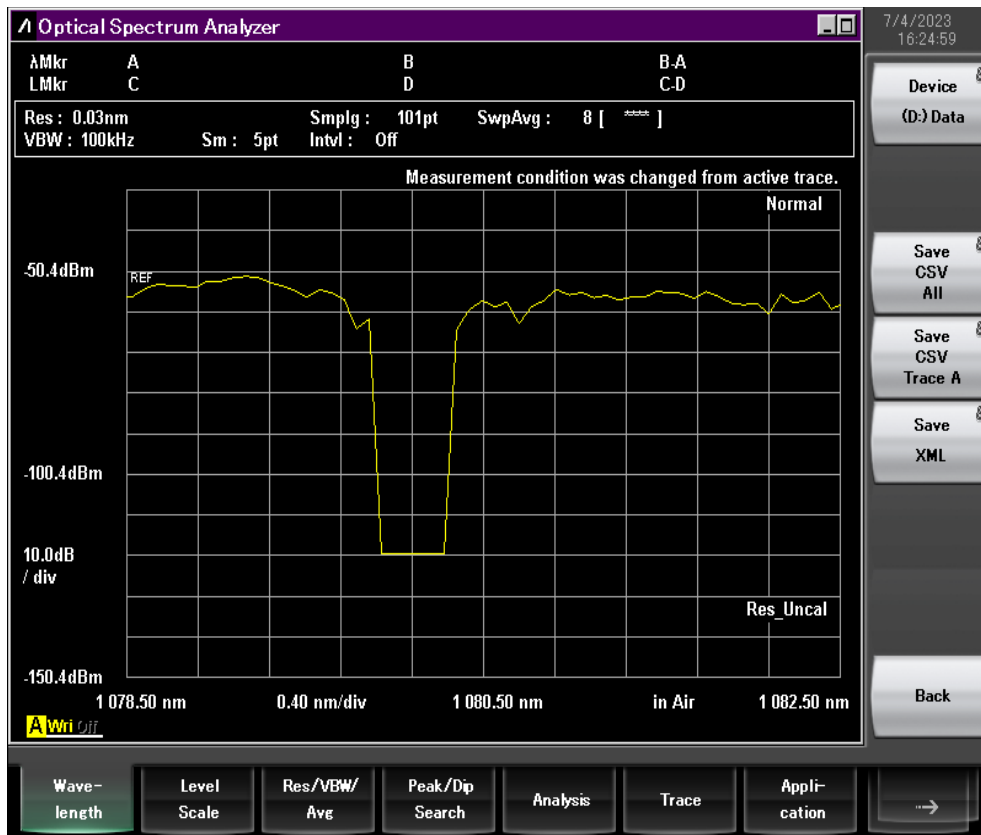(a) G1 Bragg grating



(b) G2 Bragg grating

*Fig. 7. Actual fabricating results*

The modification effects of fiber Bragg gratings are obtained through optical spectrum analyzer in Fig. 8. The transmission spectrum of G1 Bragg grating is shown in Fig. 8(a). The actual central wavelength is 979.372 nm and

bandwidth is 0.25 nm. The transmission spectrum of G2 Bragg grating is shown in Fig. 8(b). The actual central wavelength is 1080.1 nm and bandwidth is 0.52 nm.

(a)    Transmission spectra of G1 Bragg grating



(b) Transmission spectra of G2 Bragg grating

*Fig. 8. Transmission spectra of fiber Bragg Gratings (color online)*

The center wavelength of G1 Bragg grating offsets 0.628 nm with design specification. Its bandwidth deviates 0.02 nm with design value. Similarly, the center wavelength of G2 grating offsets 0.1 nm, and the bandwidth deviates 0.03 nm. Actual results are in good agreement with design results. Another, reflectivity (R) of fiber Bragg gratings can be calculated by formula $R=1-10^{(-T/10)}$ [36]. Here, T is total transmission depth. It can be seen that transmission depth T is clearly greater than 60 dBm, so reflectivity is almost 100%.

Then, fiber Bragg grating is placed into a high and low temperature box, and broadband light source and optical spectrum analyzer are placed outside the box. The temperature range is -20 $^{\circ}$C ~ 70 $^{\circ}$C and the number of cycles is 3. The changes of reflectivity, bandwidth, and center wavelength are recorded every 5 $^{\circ}$C in Fig. 9. As temperature increases, the value of central wavelength increases. The center wavelength offset ratio is approximately 0.0118 nm/$^{\circ}$C for G2 Bragg grating. Correspondingly, the center wavelength offset ratio is approximately 0.012 nm/$^{\circ}$C for G1 Bragg grating in Fig. 9(a).



(a)    The relationship between temperature and center wavelength



(b)    The relationship between temperature and reflectivity



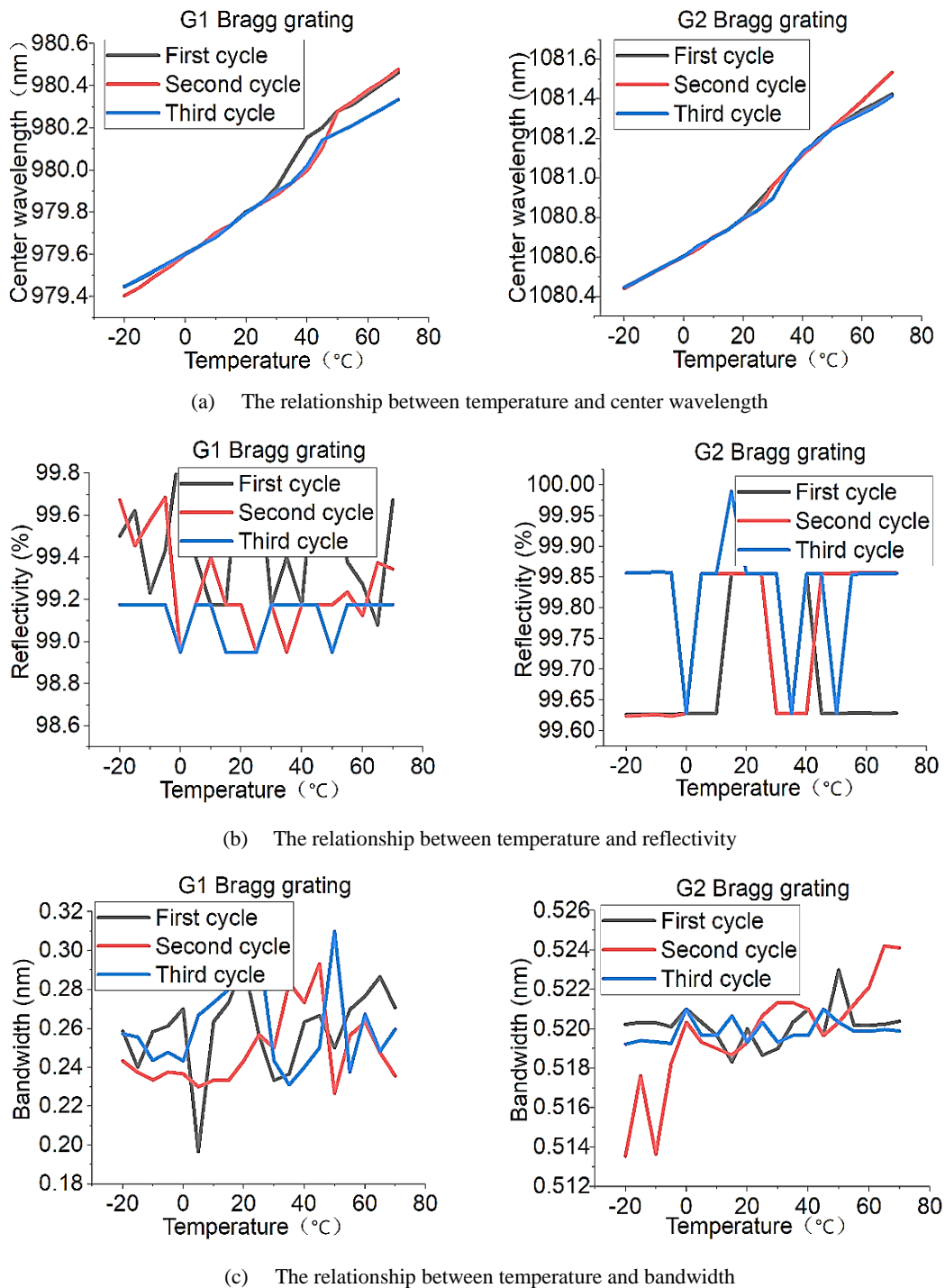(c)    The relationship between temperature and bandwidth

Fig. 9. The relationship between temperature and various parameters (color online)

Although their reflectivity fluctuate up and down with temperature increase in Fig. 9 (b), they are basically above 99%. The center wavelength drift coefficient with temperature and its linearity measured by multiple experiments are relatively stable. Similarly, their bandwidths fluctuate up and down with temperature increase in Fig. 9 (c). The maximum of bandwidth is 0.5213 nm and minimum of bandwidth is 0.5184 nm for G2 Bragg grating. And, the maximum of bandwidth is 0.31 nm and minimum of bandwidth is 0.195 nm for G1 Bragg grating.

The bandwidth and reflectivity of fiber Bragg gratings hardly fluctuate with temperature. And, bandwidth and reflectivity have good repeatability in multiple experiments.

## 5. Conclusions

In this paper, two kinds of gradient index fiber Bragg gratings are designed. Center wavelength is 980 nm, bandwidth is 0.23 nm and period is 0.32 μm for G1 Bragg grating. Center wavelength is 1080 nm, bandwidth is 0.49 nm and periods is 0.36 μm for G2 Bragg grating. Their lengths are 5 mm, and their reflectivity are greater than 99%. Composite manufacturing method is used in the fabrication process. Laser focus is shaped into an approximate cylindrical shape, which is 0.06 μm×1 cm. Then, core of fiber is induced. The test results show that center wavelength of G1 Bragg grating is 979.372 nm and its bandwidth is 0.25 nm. The center wavelength of G2 Bragg grating is 1080.1 nm and its bandwidth is 0.52 nm. Their grating lengths are slightly greater than 5 mm, and their reflectivity are also greater than 99%. The center wavelength of G1 Bragg grating is offset 0.628 nm and deviation of bandwidth is 0.02 nm. The center wavelength of G2 Bragg grating is offset 0.1 nm, and deviation of bandwidth is 0.03 nm. After high and low temperature testing, center wavelength offset ratio is approximately 0.0118 nm/$^{\circ}$C for G2 Bragg grating. The center wavelength offset ratio is approximately 0.012 nm/$^{\circ}$C for G1 Bragg grating. These fiber Bragg gratings have good performance, which are basically consistent with design specifications. The composite manufacturing methods is feasible.

### References

[1] L. Xiong, Y. X. Guo, J. J. Zhu, Measurement **209**, 112498 (2023).
[2] M. Bonopera, Materials **15**, 5561 (2022).
[3] J. He, B. J. Xu, X. Z. Xu, C. R. Liao, Y. P. Wang, Photonic. Sens. **11**, 2 (2021).
[4] H. Y. Guo, M. Xiang, Y. Hu, G. H. He, J. G. Tang, D. Fan, W. B. Gan, L. Y. Ding, Y. M. Xu, D. S. Jiang, Opt. Fiber Technol. **72**, 102955 (2022).
[5] R. Y. Lu, X. Yue, Q. Ch. Yang, E. L. Song, B. Peng, Y. Ran, Opt. Express **32**, 6 (2024).
[6] S. J. Mihailov, H. M. Ding, C. Hnatovsky, R. B. Walker, P. Lu, M. D. Silva, Photonics **10**, 625 (2023).
[7] W. J. Bao, S. Liu, W. J. Feng, Y. P. Wang, Sensors **20**, 7004 (2020).
[8] H. Ahmad, N. A. Roslan, M. K. A. Zaini, M. Z. Samion, Optik **291**, 171383 (2023).
[9] Y. H. Ma, X. Sun, X. L. Si, L. Peng, H. Wang, Y. F. Zhu, L. F. Wu, L. Yi, L. M. Li, X. Y. Zhao, C. Jiang, C. B. Mou, Y. Q. Liu, Opt. Commun. **516**, 128286 (2022).
[10] A. Rybaltovsky, S. Popov, D. Ryakhovskiy, A. Abramov, A. Umnikov, O. Medvedkov, V. Voloshin, A. Kolosovskii, I. Vorobev, Y. Chamorovskiy, D. Lipatov, Photonics **9**, 840 (2022).
[11] B. Rente, A. Mello, R. Allil, M. M. Werneck, S. S. Camargo, J. Vac. Sci. Technol. **37**, 031502 (2019).
[12] S. J. Mihailov, C. Hnatovsky, N. Abdukerim, R. B. Walker, P. Lu, Y. Xu, D. Grobnic, Sensors **21**, 4 (2021).
[13] W. Zhang, W. Zhuang, M. L. Dong, L. Q. Zhu, F. Y. Meng, IEEE Sens. J. **19**, 14 (2019).
[14] X. P. Pan, Q. Guo, Y. D. Wu, S. R. Liu, B. Wang, Y. S. Yu, H. B. Sun, Opt. Lett. **46**, 9 (2021).
[15] J. He, R. X. Chen, X. Z. Xu, J. He, B. J. Xu, S. Liu, C. R. Liao, D. J. Liu, Y. Gong, Y. P. Wang, J. Light Technol. **40**, 16 (2022).
[16] K. Madeikis, K. Viskontas, R. Danilevičius, A. Michailovas, Opt. Fiber Technol. **65**, 102636 (2021).
[17] Y. Zheng, J. Zhuo, P. Zhang, Constr. Build Mater. **304**, 124659 (2021).
[18] M. T. Wang, X. F. Cai, Y. B. Lu, A. Noori, F. M. Chen, L. B. Chen, X. Q. Jiang, Engineering Failure Analysis **146**, 107006 (2023).
[19] J. Y. Zhou, Q. Li, J. S. Xu, C. F. Li, G. C. Guo, Acta Phys. Sin. **71**, 6 (2022).
[20] F. F. Li, X. Y. Zhou, K. B. Zhang, Z. H. Shi, J. Z. Chen, X. Ye, W. D. Wu, B. Li, Acta Phys. Sin. **70**, 19 (2021).
[21] V. M. Chudnovskii, A. A. Levin, V. I. Yusupov, M. A. Guzev, A. A. Chernov, Int. J. Heat Mass. Transf. **150**,

119286 (2020).

[22] H. Choi, C. C. Young, Constr. Build Mater. **271**, 121910 (2021).

[23] P. Somers, Z. H. Liang, J. E. Johnson, B. W. Boudouris, L. Pan, X. F. Xu, Light Sci. Appl. **10**, 1 (2021).

[24] B. N. Shi, L. G. Yu, X. Y. Liang, Opt. Express **31**, 20 (2023).

[25] D. Grobnic, C. Hnatovsky, S. Dedyulin, R. B. Walker, H. Ding, S. J. Mihailov, Sensors **21**, 4 (2021).

[26] P. Arjun, V. K. Bidhun, U. K. Lenin, V. P. Amritha, Ribin Varghese Pazhamannil, P. Govindan, Mater. Today **62**, 14 (2022).

[27] Ç. Yılmaz, H. Q. Ali, M. Yıldız, Polym. Compos. **44**, 5 (2023).

[28] C. Zhu, A. Osalman, J. Huang, J. Appl. Phys. **133**, 16 (2023).

[29] Y. Zhang, Y. Lian, Sensors **23**, 11 (2023).

[30] V. Slavchev, A. Dakova, I. Bojikoliev, D. Dakova, L. Kovachev, J. Optoelectron. Adv. M. **22**(9-10), 445 (2020).

[31] C. B. Doñate, A. M. Fernández, J. Lancis, V. G. Mínguez, Photonics Res. **7**, 11 (2019).

[32] D. Kühn, A. Treffer, F. Wyrowski, R. Grunwald, Opt. Lett. **47**, 4 (2022).

[33] E. Papagiakoumou, E. Ronzitti, V. Emiliani, Nat. Methods **17**, 571 (2020).

[34] P. Somers, Z. Liang, J. E. Johnson, B. W. Boudouris, L. Pan, X. F. Xu, Light Sci. Appl. **10**, 199 (2021).

[35] M. Mounaix, N. K. Fontaine, D. T. Neilson, R. Ryf, H. S. Chen, J. C. A. Zacarias, J. Carpenter, Nat. Commun. **11**, 5813 (2020).

[36] M. Raguse, S. Klein, P. Baer, M. Giesberts, M. Traub, H. D. Hoffmann, Opt. Continuum **1**, 5 (2022).

_____

[*]Corresponding authors: dun.liu@hbut.edu.cn;
lubowen@everfoton.com